ELSEVIER

Journal of Chromatography A. 786 (1997) 333–345

JOURNAL OF CHROMATOGRAPHY A

Noise and baseline disturbances in indirect UV detection in capillary electrophoresis

X. Xu, W.Th. Kok, H. Poppe*

Amsterdam Institute for Molecular Studies (AIMS), Laboratory for Analytical Chemistry, University of Amsterdam, Nieuwe Achtergracht 166, 1018 WV, Amsterdam, The Netherlands

Received 26 February 1997; received in revised form 16 May 1997; accepted 27 May 1997

Abstract

In capillary electrophoresis (CE) with indirect detection, one is frequently confronted with low-frequency noise, occurring besides the instrumental noise that is dependent on the inherent qualities of the detector. Often wavy baseline disturbances, as well as disturbances resembling real peaks are observed. This non-detector noise type, which often shows repeating profiles, leads to a dramatic decrease in the quantitative reliability when using indirect detection. It was found that the non-detector noise originates from Joule heat production and non-uniform thermostatting along the capillary, which affect the electrophoretic transport process of ions in the background electrolyte (BGE) and consequently lead to a fluctuation of the visualizing ion concentration in the capillary. It is shown that disturbances are generated by so-called thermal nodes along the capillary, at the moment that the current is switched on. The number and mobilities of disturbances starting from each thermal node are equivalent to those of system zones, which are inherent to the BGE. The disturbances can reach the detector from the injection or the grounded side of the capillary. The magnitude of a disturbance is dependent on the thermal characteristics of the thermal node and on the composition of the BGE. Low-frequency noise, on the other hand, is generated from a multitude of small thermal nodes existing at the start of the electrophoresis or appearing newly during the CE process.

Keywords: Detection, electrophoresis; Indirect detection; UV detection; Baseline disturbances; Noise; Computer simulations

1. Introduction

Indirect detection is often used in capillary electrophoresis (CE) for the analysis of chemical compounds with an inherent lack of analytically useful detection properties [1]. The method has been described for (UV) absorption detection [2–4] and for laser-induced fluorescence (LIF) detection [5]. Both modes are based on the displacement by an analyte of a visualizing or monitoring ion present in the background electrolyte (BGE), which yields a decrease in the background signal.

Since a UV detector is present in all commercial CE instruments, and an UV absorbing ion with suitable optical and electrophoretic properties is often easy to find, indirect UV detection is commonly the choice in CE.

Generally, indirect absorption detection is performed with the concentration of the visualizing ion in the range of 2–20 m*M*. Lower concentrations are unfavorable because of the increasing peak broadening due to electromigration dispersion. On the other

*Corresponding author.

0021-9673/97/$17.00
PII S0021-9673(97)00616-X

hand, too high concentrations may affect the linearity of detection and the noise level. Also, the increased heat dissipation, already undesirable in itself, leads to increased noise, as will be discussed at length in this paper.

Rather extensive work has been carried out to characterize and optimize the signal-to-noise ratio in indirect detection schemes [6–10].

The subject of this work is the important observation [11–13] that the noise in indirect UV absorption system is often much larger than can be expected on the basis of instrumental specifications. It appears that the total background noise is often dominated by the non-instrumental contributions. It is generally observed that the magnitude of the additional noise depends strongly on the CE conditions such as the BGE composition, the dimensions and nature of the inner surface of the capillary, the thermal conditions, instrumental configurations, the voltage, and is difficult to predict.

Wang and Hartwick [11] indicated that this additional noise mostly reflects real changes in the concentration of the visualizing ion c_{vis}, although the mechanism remained unknown. In a few papers the additional noise was attributed to the adsorption and desorption of the visualizing ion to and from the wall of the capillary [3,8]. Also, perturbations such as an immersion peak and a spontaneous-marker peak transported at the rate of electroosmotic flow were attributed to phenomena occurring at the capillary inlet [14,15]. In one paper [16] the amplitudes of the electric current and baseline fluctuations were related to fluctuations of the buffer temperature and it was assumed that the fluctuations resulted from the temperature dependence of the refractive index of water.

In a previous work [12], we discussed the heat dissipation as a possible cause for this type of noise. In the present paper, we attempt to shed more light on this matter and to give possible strategies to minimize it.

2. Experimental

2.1. Apparatus

Experiments were carried out using an ABI capillary electrophoresis system, Model 270A-HT (Foster City, CA, USA), which is equipped with an UV detector. Fused-silica capillaries of 75 μm I.D. and 350 μm O.D. (Polymicro Technologies Phoenix, AZ, USA) were used, unless stated otherwise, with a total tube length of 0.70 m and with a detection window at 0.50 m distance from the injection end.

Electropherograms were recorded and analyzed on a personal computer with an appropriate ADC card and interface, using the electrophoresis data processing software CAESAR 4.0 (Lauer Labs, Emmen, Netherlands), at a detector rise time setting of 1 s. and a data sampling rate of 5 Hz. In all electropherograms shown the absorbance decreases from bottom to top, as is often the case when indirect detection is applied.

The UV spectrum of a compound was measured by a UV–Vis scanning spectrophotometer, Model PU 8720 (Pye-Unicam, Cambridge, UK).

2.2. Chemicals

Picric acid (PA) (0.5 ml H_2O/g), toluenesulphonic acid (TSA), 6-aminohexanoic acid, trimethoxy-ammonium (Tris), histidine (L), 1-pentanesulphonic acid sodium salt (PSA), and N-cetyl-N,N,N-trimethyl-ammonium bromide (CTAB) were obtained from Merck (Darmstadt, Germany); glycine and 3-amino-propanol from Sigma (Bornem, Belgium); sorbic acid from BDH (UK).

2.3. BGE and sample solutions

Unless stated otherwise, 10 m*M* PA was used as the visualizing agent for indirect detection. BGEs were prepared by mixing PA with an appropriate amount of a pH buffer: glycine, 6-aminohexanoic acid, histidine, Tris and 3-aminopropanol at pH 2.5, 4, 6, 8.2 and 10, respectively and NaOH at pH 11.6, 12.1 and 12.6. When necessary, HCl and more base were added to increase the conductivity of the BGE without changing in the buffer pH. The injection solution was 0.2 m*M* PS dissolved in the running BGE.

2.4. Procedures

Unless stated otherwise, the following conditions

were used. The voltage applied was +14 kV when the pH of the BGE was >4 and −14 kV otherwise. The sample was injected by applying vacuum of 167 mB for 0.5 s, 1.2 s and 4.5 s, for capillaries with I.D. of 75, 50 and 25 μm, respectively, to keep the amount of the analyte injected the same. The UV detector was operated at 357 nm. The temperature in the ventilation area was 30°C and at ambient temperature (21±2°C) in the other parts of the CE system.

The detector baseline noise was measured while flushing the capillary with BGE, without current. The background noise was measured with the BGE with an applied voltage of 14 kV, without flushing. The peak-to-peak noise, N_{XX} in the noise records were measured for at least 10 min continuously on a steady baseline.

2.5. CE simulation with the computer program IMPULSE

The program IMPULSE [4,12,17–19] was used for the prediction of the number and the mobilities of system zones that are inherently related to a BGE. The pK_a values to be entered in the program were obtained from literature. Mobilities were taken from literature (see Table 1), measured experimentally or estimated from the properties of a constituent. Normally, they are sufficiently accurate to allow the prediction of the system zones, because the properties of a system zone are mainly dependent on the composition (concentrations) of the BGE and not very sensitive to errors of a few percent in the mobility values. The rate of electroosmotic flow (EOF) was commonly measured by the 'water' system peak, i.e. effective mobility equal to zero [18], in indirect detection. When the EOF was too small, it was indirectly determined by measuring the apparent mobility ('apparent' is used in this paper for indicating the total mobility, including the effect of electroosmotic flow) of the analyte PSA.

All mobilities in this paper are expressed in the units of 10^{-9} m^2 V^{-1} s^{-1}.

3. Results and discussion

3.1. General

All used data on the pertinent ions are collected in Table 1. The analyte and the visualizing ions are singly charged strong ions at all pH values investigated and their mobilities match. In this way any possibly occurring irrelevant effect, e.g. from acid–base reactions and the signal intensity change due to electrophoretic overloading effect were excluded and the transfer ratio, TR, is very close to 1 under most conditions [20]. In most cases PA (ϵ=8600 AU/m/

Table 1
Data with respect to BGE components and the analyte

Compound	pK_a	Ionic mobility ($\cdot 10^{-9}$ m^2 $V-1$ s^{-1})
Picric acid (PA)	0.4	−31.5
Toluenesulphonic acid (TSA)	−2	−31.2
Pentansufonic acid (PSA)	−2	−32.19 ±0.01[a], n=4
Glycine	2.3, 9.6	+37, −37
6-Aminohexanoic acid	4.4, 10.8	+27, −27[b]
Histidine	6.0, 9.3	+29.6, −28.8
Tris	8.2	+28[b]
3-Aminopropanol	10.0	+35[b]
Carbonic acid	6.4, 10.3	−46, −72
Cl^-	–	−75[c]
Na^+	–	+52[c]

All values were collected from literature ([22–26]).
[a] For the measurement of the EOF in a small value; precisely determined at 30°C with the BGE consisting of 10 mM PA and 50 mM glycine at pH 3.0 (conductivity 0.1 Ω^{-1} m^{-1}).
[b] Estimated according to the charge and the size of the ion.
[c] Measured experimentally. For details see Section 2.

μM), λ_{max}=357 nm) was used rather than TSA (ϵ=23 000, λ_{max}=197 nm); the advantage being that PA can be measured at a high wavelength at all pH values, without interference from other components in the BGE.

3.2. Detector noise

In this paper detector noise, N_{det}, is defined as the peak-to-peak value of random fluctuations in the baseline observed when no voltage is applied. The frequency of the noise, estimated as the number of times that the background signal crosses the baseline per minute, is higher than 40/min with the present detector at a detector rise time of 1 s at a data sampling rate of 5 Hz. N_{det} is believed to originate from electronic and optical imperfections, thermal noise and photocurrent shot noise.

We have found, as shown in Fig. 1, that N_{det} is strongly dependent on the wavelength. With the present deuterium lamp, a low detector noise is achieved in the range 220–280 nm. The noise measured using a capillary of 75 μm I.D. flushed with water is minimal ($5 \cdot 10^{-5}$ AU) at ~240 nm.

Although the detector noise depends on the absorbance of the solution, this dependency was found to be weak. When for instance the absorbance level was increased with sorbic acid or PA from 0 to 0.6 AU in a 50-μm capillary, the noise measured changed from $4 \cdot 10^{-5}$ to $6 \cdot 10^{-5}$ AU at 256 nm and from $1 \cdot 10^{-4}$ to $1.4 \cdot 10^{-4}$ AU at 357 nm, respectively.

The noise increased by a factor of two when the capillary inner diameter was changed from 25 to 75 μm.

Under ideal conditions, only detector noise would be observed. Therefore, detector noise sets the ultimate limit to the performance. The limit of detection in terms of concentration, c_{LOD}, under these conditions can be predicted by Eq. (1):

$$c_{LOD} = kN_{det}/(TR\epsilon b) \quad (1)$$

where k is a statistical factor ($\approx$2), of which the value is somewhat uncertain as a result of the definition of N as a peak-to-peak value, ϵ is the molar absorptivity of the visualizing ion and TR is the transfer or displacement ratio.

As detector noise is a function of the wavelength and of the capillary inner diameter, one has to be careful in the use of Eq. (1) as a guide for the choice of conditions to obtain a lower c_{LOD} (Fig. 1).

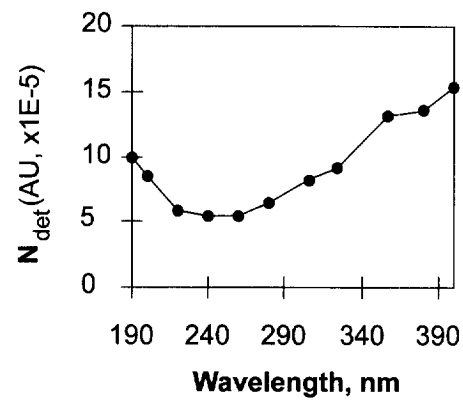

Fig. 1. Detector noise as a function of the wavelength for a 75-μm capillary.

3.3. Baseline fluctuations when passing current

The commonly observed types of fluctuation in the background signal have been categorized with the help of Fig. 2:

- N_{det}: detector noise, the instrumental noise discussed above, also observed with the voltage off;
- N_{low}: low frequency noise, additional noise, random, occurring throughout with a frequency of 2–10/min;
- D: disturbances including the electroosmotic flow (EOF) peak, with a repeatable shape and position;
- S: sample peaks.

The combination of detector and low frequency noise forms the background noise N_{bg}. N_{low} can be easily extracted from background noise by filtering out the high frequency detector noise with the data processing software. Both N_{low} and D are considered as non-detector noise in a broad sense. They can be even orders of magnitude larger than the detector noise and are the subject of this paper.

In preliminary experiments detectors, power supplies and CE set-ups from various sources were tested and compared with respect to the non-detector noise. Results showed no significant differences when changing power supplies or detectors. However, we found that the configuration with respect to the heat dissipation of a capillary did have a large

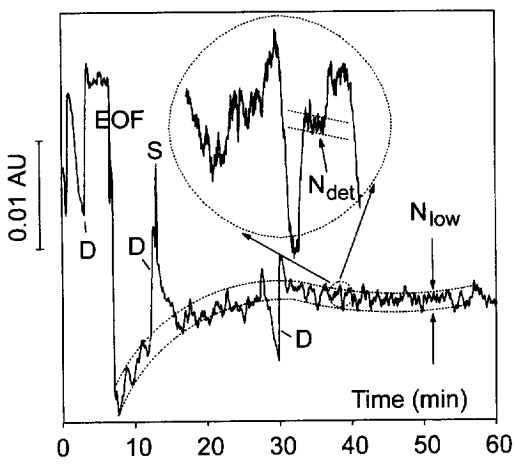

Fig. 2. Classification of baseline fluctuations in an electropherogram. See text for the definitions. Conditions: BGE: PA 10 m*M*, 3-aminopropanol ($pK_a = 10$) 43 m*M*, HCl 11.3 m*M* (pH 10), conductivity 0.19 Ω^{-1} m^{-1}; capillary: 0.5/0.7 m×75 μm; Injection: 0.2 m*M* PSA in BGE, 167 mB/0.5 s. Electrophoresis: +14 kV, 19 μA; 30°C in the ventilation chamber; Indirect detection: 357 nm; mobility of EOF: $62.0 \cdot 10^{-9}$ m^2 V^{-1} s^{-1}.

influence on the non-detector noise. In a previous work [12] it has been shown that the repeating profiles of disturbances were different from condition to condition as well as from CE set-up to set-up. Of the various equipments tested, the ABI instrument gave the smallest noise and disturbances among the set-ups tested. The configuration of the ABI CE system with respect to thermal conditions is shown in Fig. 3.

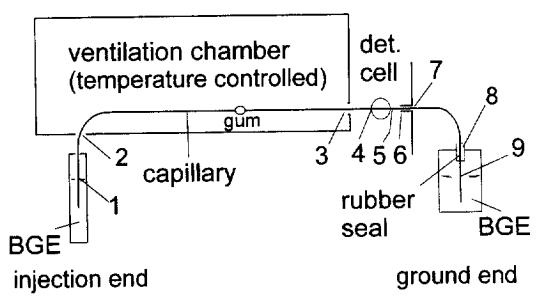

Fig. 3. Heat dissipation features of the CE set-up. Thermal nodes 1–4 are at positions 480, 460, 60 and 10 mm from the detection area, respectively. Thermal nodes 5–9 are at positions 10, 32, 67, 155 and 190 mm from the detection area, respectively. The gum applied in some experiments was located 250 mm from the inlet. Positions where the temperature differences may occur are indicated with numbers.

We have been experimenting with many systems. Rather than reporting on each individual experiment, we summarize trends and characteristics observed for non-detector noise resulting from passing a current, giving illustrations with figures where that seems appropriate:

(a) Disturbances (*D*) often have repeatable positions and shapes in the electropherogram.

(b) The disturbances (*D*) occur exclusively in a certain time window after an injection has been made or after the voltage has been switched on, i.e, when the system is left under constant voltage the disturbances disappear after a time lapse comparable to the duration of an electropherogram.

(c) Low frequency noise (N_{low}) and disturbances (*D*) show different profiles when changing the polarity of the voltage.

(d) Low frequency noise (N_{low}) goes up rather regularly with the current, irrespective whether the higher current is caused by a high voltage or by a high conductivity; see Fig. 4a.

(e) For the disturbances the same trend is observed, but the specific composition of the BGE is also of great importance; see Fig. 4b. Both N_{low} and *D* appear to have no direct relation with the pH.

(f) When the conductivity is varied independently from the visualizing ion concentration, the noise is always largest at the highest conductivity; see Fig. 5a. For the particular solute used here (matching the visualizing ion nearly exactly in mobility) the signal hardly depends on these conditions, as TR is always equal to 1. This explains why the ratio S/N_{low}, given in Fig. 5b, is only weakly dependent on the value of c_{vis}.

(g) Low-frequency noise (N_{low}) increases with increasing capillary inner diameter much more rapidly at a high conductivity than at a low conductivity; see Fig. 6. Changing the capillary inner diameter from 25 to 50 and then to 75 μm, the signal increases in a ratio of approximately 1:2:3, as expected. However, the noise is increasingly stronger, resulting in an actual deterioration of the signal-to-noise ratio.

(h) The signal-to-noise ratio is not always improved by using a visualizing ion with higher molar absorptivity, ϵ. This is shown in Fig. 7, where different values of ϵ were obtained by measuring PA at different wavelengths (284–357 nm). At low

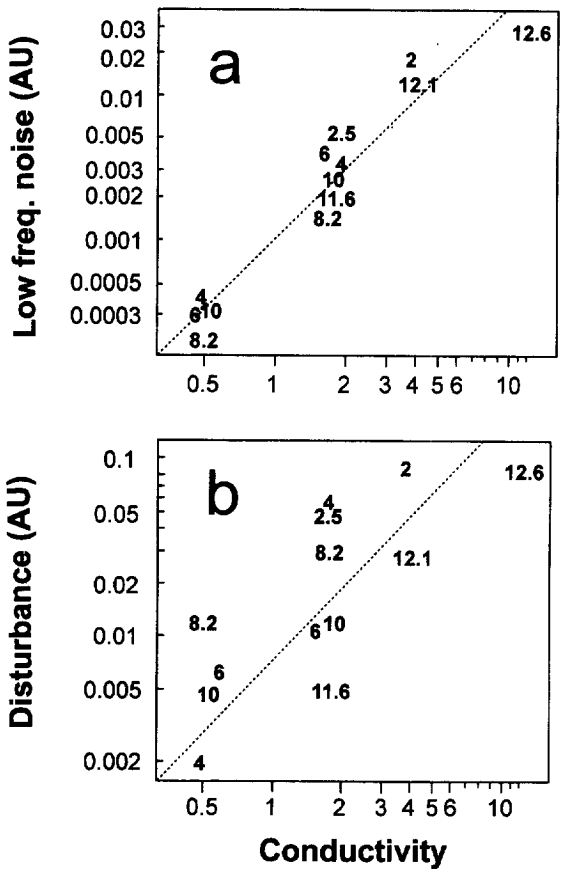

Fig. 4. Magnitude of disturbances (a) and low-frequency noise (b) as a function of the conductivity (in units 0.1 $\Omega^{-1}\,m^{-1}$) of the BGE in indirect detection (357 nm). The pH values of the BGEs are indicated by numbers in the plot. Capillary: 75 μm I.D.; voltage: +14 kV; 30°C in the ventilation chamber; without sample injection.

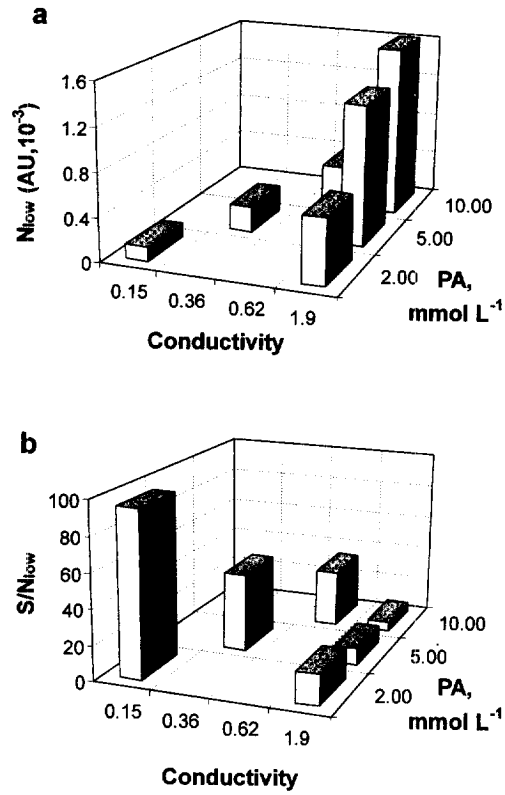

Fig. 5. Influence of the conductivity (in units 0.1 $\Omega^{-1}\,m^{-1}$) and the concentration of the visualising ion (PA) on signal and low-frequency noise.

conductivity (line 1), where N_{det} predominates, the signal-to-noise ratio increases linearly with the value of ϵ. However, at high conductivity (other lines), where other types of noise are present, the signal-to-noise ratio becomes almost independent of the value of ϵ.

(i) When low frequency noise predominates, there is no advantage in using a bubble cell capillary instead of a normal one because the noise and the analyte signal increase in the same proportion. This is illustrated in Fig. 8.

(j) The temperature in the ventilation area of the CE system has a strong influence on the low frequency noise and disturbances (Fig. 9).

3.4. Origin of disturbance peaks

In view of the general observations mentioned above, it is likely that the low frequency noise and the disturbances are closely related to the Joule heat generated in the capillary, to the heat dissipation efficiency and to the thermostatting condition of a CE system. Fig. 10 illustrates the base-line traces obtained, without doing an actual injection, but after interruption of the voltage as if an injection had been made, with three different thermostatting conditions. The first of these is the regular set-up, the second consisted of an air ventilated sheathing tube fitted

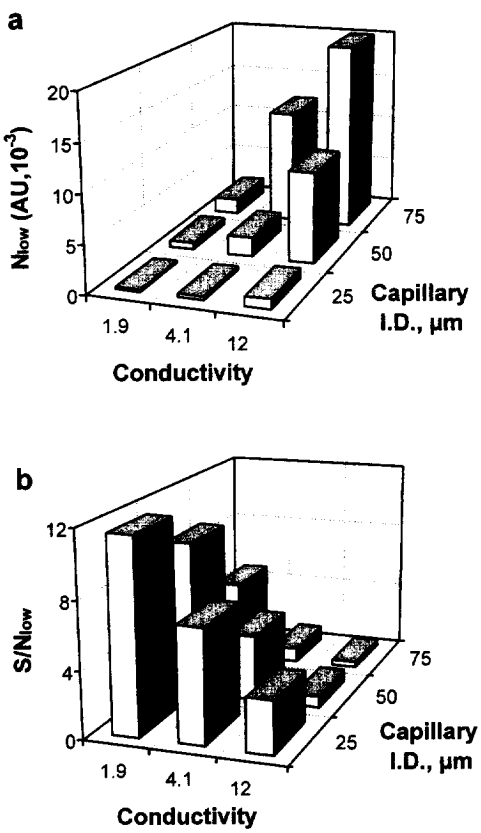

Fig. 6. Influence of the conductivity (in units 0.1 Ω^{-1} m^{-1}) and the capillary I.D. on signal and low-frequency noise. BGE: 10 m*M* PA with Tris (pH 8.2) or NaOH (pH 12.1 and 12.6) when the conductivity of the BGE is 0.19, 0.41 and 1.2 Ω^{-1} m^{-1} respectively. Other conditions as in Fig. 2.

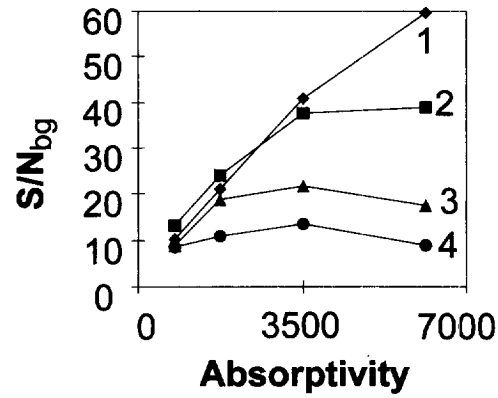

Fig. 7. S/N_{bg} versus the absorptivity of the BGE at different conductivities, κ, (Ω^{-1} m^{-1}) and visualising ion concentrations, c_{vis}, (m*M*) of 1: κ=0.013, c_{vis}=2; 2: κ=0.032, c_{vis}=5; 3: κ=0.19, c_{vis}=2; 4: κ=0.19, c_{vis}=5, respectively. CE conditions: as in Fig. 2. Different absorptivities are obtained by measuring PA at different wavelengths.

around the capillary. In the third a similar sheathing tube was flushed with water.

It is seen in the figure that the base line with the regular set-up is dominated by disturbances occurring before 24 min, while the low-frequency persists also after that moment. With the forced-air cooling system (Fig. 10b), some disturbances and low-frequency noise are largely suppressed. They are even more reduced with the water cooling system (Fig. 10c). The larger high-frequency noise in Fig. 10c probably results from the current leakage through the water channel in the sheath to the body of the CE instrument, as witnessed by a very small electric discharge sound heard inside the separation chamber.

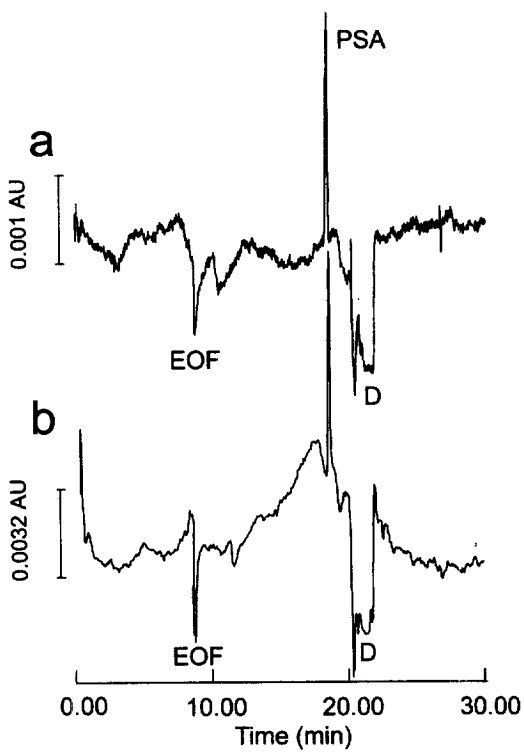

Fig. 8. Comparison of the electropherograms obtained with a normal 25-μm I.D capillary (a) and a bubble cell capillary of approximately 150 μm in diameter at the bubble position (b).

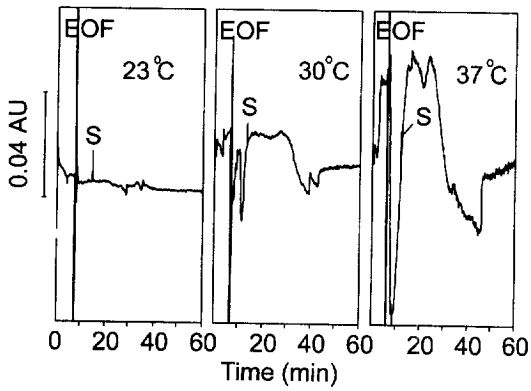

Fig. 9. Influence of the operating temperature on disturbances and low-frequency noise.

This experiment as shown in Fig. 10 clearly demonstrates the influence of the thermal conditions.

Surprisingly, two disturbances, D_1 and D_2, remain with the two modified cooling systems. We believed that these originate at the positions where thermal conditions are less favorable. These occur at the ends of the cooling tube and the injection part of the capillary (see Fig. 11). This aspect has been further investigated by means of the following experiment.

Any part of the capillary having a thermal regime different from that in the main part of the capillary will be called a thermal node. The differences can be caused either by surroundings that differ in temperature (such as occurs at the inlet and outlet of the temperature controlling chamber) or by differing heat transfer rates (such as occurs at the boundaries, in the surrounding of the capillary, between solid–liquid–air and stagnant air–moving air).

In order to demonstrate the role of thermal nodes, one was introduced deliberately in the CE system shown in Fig. 3. This was done by applying a piece of gum to the capillary (covering about 0.02 m), 0.25 m away from the injection end. The electropherog-

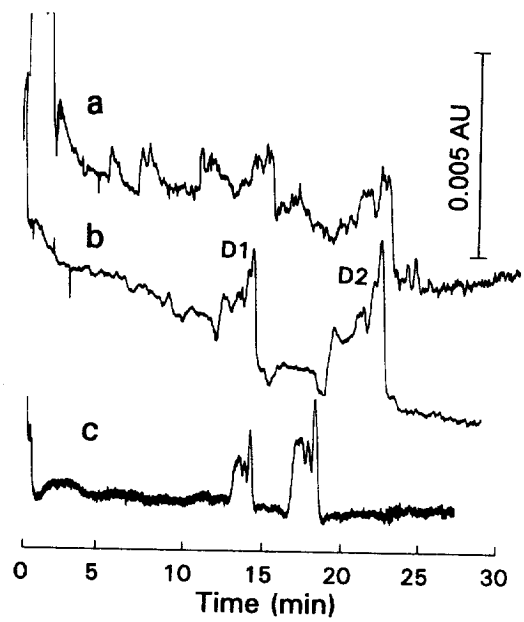

Fig. 10. Disturbances and low-frequency noise under different thermostatting conditions. (a) Conventional system with ambient temperature in the ventilation chamber; (b) modified system with the capillary sheathed with a plastic tube flushed with ambient air; (c) sheathing tube flushed with tap water (~18°C). CE conditions: BGE: 5 m*M* toluenesulfonic acid+29 m*M* glycine (pH 3.0); capillary: 0.90/0.70 m×75 μm; electrophoresis: +28 kV; indirect detection: 195 nm.

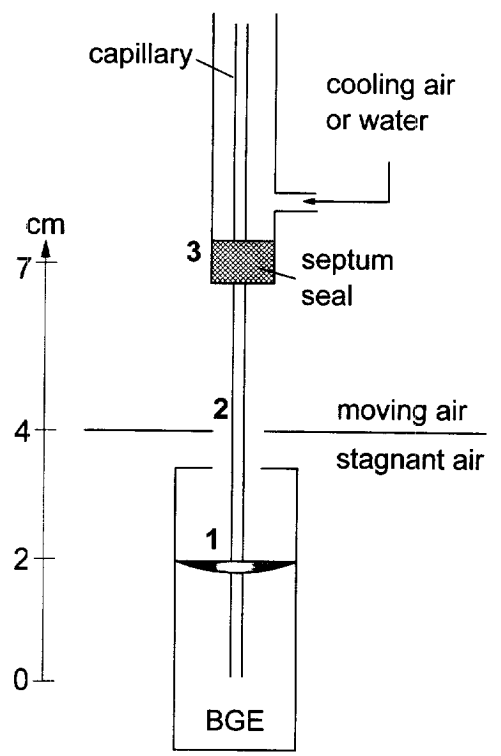

Fig. 11. Details of the injection part of the CE set-up modified with a cooling tube as in Fig. 10b and c. Thermal-nodes in this part are indicated with numbers.

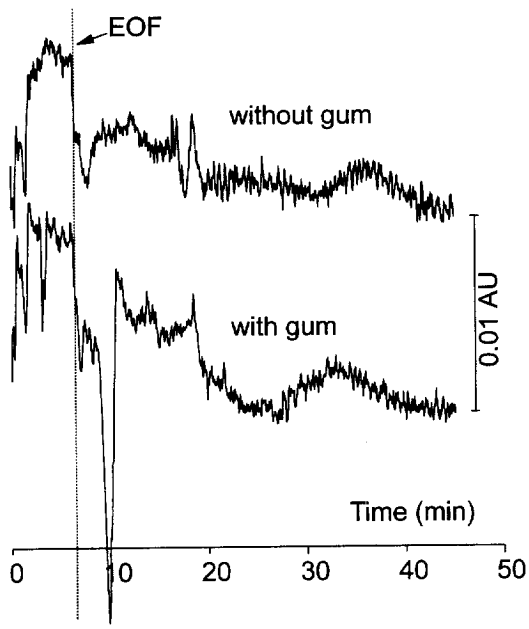

Fig. 12. Electropherograms with and without a gum disturbance as in Figs. 3 and 11a. CE conditions: without analyte injections; rest as in Fig. 2 but with fresh BGE.

ram obtained under such conditions is shown in Fig. 12. Two new disturbance peaks (at 3.2 min and 9.8 min) were observed. In order to show that the deviating temperature at the gum position generated real concentration distributions, we applied current only for a short time, and next flushed the content of the capillary past the detection. In this way a (broadened) image of the concentration distribution within the capillary, present after termination of the current passage, was obtained. Fig. 13 shows the results. The application of the gum at 15°C (trace d) leads to a very strong disturbance. The same disturbance, however, is clearly present when the gum was initially at ambient temperature (trace c) or at the temperature of the ventilation chamber (trace b). This shows that apart from the imposed temperature also the heat transfer is important.

It is obvious that the appearance of additional disturbances (Fig. 12b) and the change of the concentration profile in the capillary (Fig. 13) result from the thermal condition at the gum position. The concentration change appeared as a (sometimes peak-like) baseline disturbance, as if a sample zone was injected at the disturbance position.

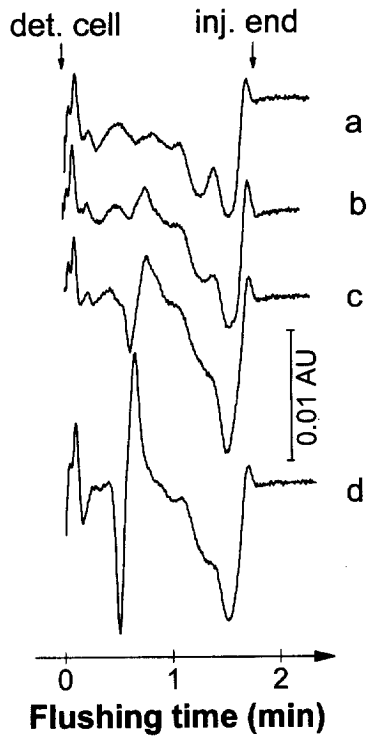

Fig. 13. Image of capillary tube content of the visualising ion obtained with the CE set-up in Fig. 3 but disturbed by sticking a piece of gum to the capillary 0.25 m away from the injection end. The image was obtained by applying current only for a short time, and next flushing the content of the capillary past the detection point. BGE conductivity $=0.19\ \Omega^{-1}\ m^{-1}$; Thermal conditions at gum position: (a) without gum; (b–e) with gum, with gum temperature being ~30°C, ambient and 15°C, respectively.

3.5. Relation to system zones

At that point we were almost sure that the disturbances are caused by thermal nodes. However, how these can generate the responses in the detector in normal operation remained a question.

A key observation in that respect was that the migration rate of the disturbances are those of the system peaks as predicted by the software used [18].

Consider first the two groups of disturbances D_1 and D_2 in Fig. 10. From the shape and position of the disturbances it can be inferred that they come from the same source as they have very similar profile. This source is most probably a part of the capillary close to the injection end by following evidence. First, the time widths of the two disturbances are

nearly 10% of their migration time, while the total length of the three thermal nodes at injection end (Fig. 11) is also 10% of the effective length of the capillary. Second, the disturbances are split into three successive peaks, that in all likelihood correspond to the three thermal nodes mentioned above. Finally, the mobilities of these disturbances are in a good agreement with those of system peaks when it is assumed that they are generated at the injection end.

To confirm that the disturbances are indeed system zones, additional experiments based on the conditions in Fig. 10b have been done. The mobilities of system peaks were changed by changing the pH of the BGE; from 3.0 to 2.7 and 3.3, respectively. Two disturbances were monitored. The software predicts two system zones will occur in these systems, with one mobility being zero and the other depending on pH. The comparison of the experiments and the computer predictions, in terms of mobilities, are listed in Table 2. The highly consistent findings confirm in our opinion that the disturbances and systems zones are related to each other.

It should be noted that most of these experiments were carried out without actual injection of any sample; the only thing done was switching the voltage on. In real electropherograms, system peaks will also be excited by the introduced sample solutions (unless these are carefully matched to the BGE in composition). These non-thermal system peaks, observed by many workers, are usually much sharper than the thermal ones discussed here. They will overlap (appear at the same time) as the thermal ones generated at the injection end, as discussed above.

Consider next, in the electropherogram of Fig. 12b, the disturbances at 3.2 min and 9.8 min, generated at another position, deliberately, by means of the gum experiments. These disturbances likewise match the computer predictions, as shown by Table 3. That is, if it is assumed that generation takes place at the gum position (0.25 m effective length), the experimental mobilities that can be assigned to them match the prediction of the software for the system peaks. In this way all other disturbances could be identified, as a combination of a point of generation and a mobility pertaining to a system peak. The points of generation are thermal nodes close to either the injection end or to the detection cell, as indicated in Fig. 3.

Table 3
Migration time of disturbances (t_D) measured and predicted with IMPULSE[a] for Fig. 12b

Disturbance no.	t_D (exp.) (min)	t_D (pred.) (min)	Starting point
1	3.2	3.2	Gum
2	9.8	9.6	Gum
3	6.4[b] (EO)	6.4	Inlet
4	19.0	19.1	Inlet

[a] Computer CZE simulation program.
[b] Refers to electroosmotic flow-rate, which is measured as $65.1 \cdot 10^{-9}\ m^2\ V^{-1}\ s^{-1}$.
Evidences that the gum sticking position is one of the sources of the disturbances.
For the predictions of t_D the mobilities given by IMPULSE were added to the experimentally found μ_{eo} values.

Fig. 14 illustrates a case where the set of disturbances is more complicated. The BGE contained 2 m*M* CTAB, so that very low EOF rates were obtained. Two system zones (A and B), with mobilities of zero and $+5.0 \cdot 10^{-9}\ m^2\ V^{-1}\ s^{-1}$, were predicted by the software. When different power polarities were applied, disturbances were passing slowly though the detector either from injection end (+14 kV) or from the terminal end (−14 kV). The

Table 2
Comparison of the mobilities of disturbances measured and of system zones predicted with IMPULSE[a]

	pH 2.7		pH 3.0		pH 3.3	
	Measured	Predicted	Measured	Predicted	Measured	Predicted
D_2 (EOF)	15.6	–	16.6	–	16.8	–
D_1 (apparent)	33.48	32.9	25.5	25.2	19.6	19.7

[a] Computer CZE simulation program.
The experiment conditions at pH 3.0 were same as in Fig. 10b and those at other pH values were obtained by changing the amount of glycine in the BGE at pH 3.0. The third peak in each disturbance was used to calculate the mobility.
Predicted values are the sum of experimentally observed μ_{eo} (from D_2) and the mobilities given by the software.

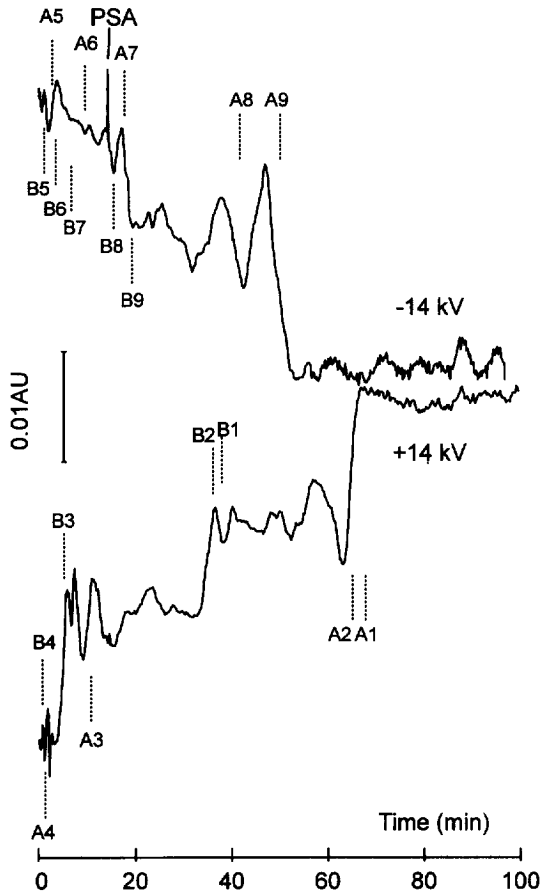

Fig. 14. Electropherograms obtained under different voltage polarities. Calculated disturbance positions are coded as follows: A and B refer to system zones of zero and 5.0 (10^{-9} m^2 V^{-1} s^{-1}), respectively; 1–9 refer to nodes as given in Fig. 3. CE conditions: BGE: 10 m*M* PA+50 m*M* glycine+0.002 m*M* CTAB as electroosmotic flow suppress agent (pH 3.0); Electrophoresis: ±14 kV, 9 μA, 30°C in the ventilation chamber; Conductivity: 0.10 Ω^{-1} m^{-1}.

identification of each disturbance, as being generated at a certain thermal node, (see Fig. 3) was made; the results are indicated with dashed lines in Fig. 14.

Disturbances can sometimes also be related to carbonate, inadvertently present in the BGE due to absorption of carbon dioxide from ambient air, either into the water used or into the BGE after its preparation. This is likely to occur in all BGEs with pH>5–6, unless special precautions are taken. According to the system zone theory, the presence of carbonate in the BGE can cause one more system zone. Such disturbances were found in the electropherograms in Figs. 2 and 9, with migration times longer than 25 min. Such additional interferences can be avoided by applying helium sparging of the water and other measures to avoid contamination with carbonate.

To conclude this section, it is necessary to discuss the mechanism by which a thermal node can generate a disturbed zone. When electrophoresis proceeds continuously in a BGE without injection of sample, there is a stationary and uniform transport of all the components: All fluxes are independent of time and position. As long as this is the case, no system zones, or zones of any kind, can develop.

When a region in the capillary is always at a higher temperature, this situation is still the same. Most components accelerate when entering this region, and some may slow down, as a result of shifting acid–base equilibria, but the concentrations in this part are in the long run automatically adapted, so that for each component the flux is again stationary and uniform. Thus, observation at a particular spot with a detector will also not reveal any changes in concentration. In other words, every ion or fluid element passing the detector zone, has 'seen' the same history. Therefore, a thermal node should be **transient** if it is to generate disturbed zones.

Zones in the BGE can develop when in a region the BGE differs quantitatively (i.e. not qualitatively; by the presence of analytes) in composition from the BGE elsewhere. However, heating up a part of the capillary will change the concentrations to only a minor extent, by thermal expansion, and in the same proportions. Therefore, it is unlikely that this would be the cause for a significant disruption of uniformity and stationarity of the fluxes.

Heating does change significantly the mobilities and may also change them to different degrees, especially when H^+ and OH^- play a role. Also, the position of various acid–base equilibria may shift, with possibly an even larger effect on the relative values of the effective mobilities. Thus, the stationary and uniform electrophoretic transport is disturbed in this manner. After cooling down to the original temperature, the disturbances have moved or might even have been resolved in several zones. The original situation is lost irreversibly.

Such transient nodes occur when switching on the

voltage (i.e. at or shortly after injection) when different parts may heat up differently or at different rates.

3.6. Origin of low-frequency noise

Although the previous sections contain a reasonable explanation of the occurrence of deterministic disturbance peaks in the electropherogram, the question of the origin of the (non-predictable) low frequency noise has not been resolved. A possible explanation could be found in a combination of many small disturbances generated from many small thermal nodes. This is supported by the fact that low frequency noise decreases considerably when using the water cooling system, as shown in Fig. 10c. Such multiple smaller thermal nodes may occur at the positions where the capillary is bent, where it is supported or fastened to parts of the set-up, or where the air flow may deviate from the average.

However, there is one important difference between low frequency noise and disturbances. The former goes on forever, after the voltage has been switched on, whereas disturbance peaks occur only within a given time frame after (we believe now that this time is determined by the 'slowest' combination of mobility and point of generation).

In order to explain the low frequency noise, it is necessary to assume that yet another type of thermal node also occurs: **fluctuating** ones, that keep changing their temperature also long after the voltage switching.

In this model, the additional low frequency noise consists of a multitude of smaller and larger system zones, generated at various positions in the capillary where the temperature has made excursions. Such excursions can be expected to result from e.g. unstable air flow.

4. Conclusion

4.1. Disturbances

This work has lead to the following conclusions regarding baseline disturbances as observed in indirect detection experiments:

(1) In addition to normal system peaks, generated by the injection of a sample solution, other disturbances are observed, that are brought about by the mere act of switching on the voltage.

(2) Each of these additional disturbances can be connected to a thermal node, at one or the other side of the detector. Whether they will be visible in the detector depends on the sign of the mobilities of system zones in the BGE; disturbances generated at the terminal ('wrong') end of the capillary obviously can become visible only when at least one system zone has an apparent mobility of a sign opposite to the regular ones in the experiment.

(3) When only one system zone exists (in a two-ion BGE, which then has zero mobility), all disturbances directly reflect the intensities, widths and positions of the thermal nodes in the part between injection point and detector.

(4) System zones with small apparent mobilities and starting from more remote thermal nodes may lead to broad disturbances which appear sometimes like a baseline drift.

(5) Better thermostatting eliminates many of these thermally induced disturbances, but not the ones originating at both end vials.

4.2. Low-frequency noise

Low-frequency noise is probably generated by non-stationary thermal nodes occurring when air-cooling is applied. The transport of the multitude of resulting disturbances follows the same mechanism as that of the system peaks and thermal disturbance: via system zones.

4.3. Reduction of non-detector noise by the optimization of CE conditions

The most effective method to avoid non-detector noise and disturbances is to eliminate instrumentally all thermal nodes in the capillary by, ideally e.g., an uniform cooling surround whole capillary everywhere. Liquid is considered as the best cooling medium. Some commercial CE system indeed use liquid as cooling medium. Our results clearly show that this forms a significant advantage in CE with indirect UV detection.

However, even there a problem remains: Thermal conditions at the injection part, detection part and

terminal vial are still less favorable. Disturbances generated there will still interfere in the electropherogram.

Another approach, that would eliminate disturbances (but probably not the low frequency noise) would be to avoid interruption of the voltage during injection. In other words, injection as in regular HPLC, where the transport is not interrupted. This would require a basic modification of the hardware in CE; one approach to realize this by means of micro-machined T-pieces has been investigated recently by van der Moolen et al. [21].

When the instrumentation is given, other approaches are indicated and worthwhile trying. They can be summarized as follows:

(1) Decrease heat production by using a BGE with a conductivity as low as possible in view of the electromigration dispersion and the requirements of the indirect detection process itself.

(2) Use a narrower capillary, but pay attention to the problems of a longer flushing time and possible loss of detection sensitivity resulting from the smaller path length.

(3) Make the BGE as simple as possible. The simpler the BGE is, the fewer system zones and disturbances can be expected. When working at higher pH than 6, try to avoid contamination of the BGE with carbonate.

(4) Try different types of co- and counter-ions with different mobilities or pK_a values in the BGE. In this way the number, position and magnitude of the system zones disturbances [12] can be manipulated, so that they interfere the least in the analysis. Fortunately, the position of system peaks can be predicted rather accurately by means of the CE simulation computer program, where as the position of analyte peaks depends – in good approximation – only on the pH.

(5) In either liquid or air cooled systems, avoid thermostat temperatures differing much from ambient temperature (in most set-ups part of the capillary is still partly influence thermally by ambient).

References

[1] E.S. Yeung, W.G. Kuhr, Anal. Chem. 63 (1991) 275A.
[2] S. Hjertén, K. Elenbring, F. Kilar, J.L. Liao, A.J.C. Chen, C.J. Siebert, M.D. Zhu, J. Chromatogr. 403 (1987) 47.
[3] F. Foret, S. Fanali, L. Ossicini, P. Bocek, J. Chromatogr. 470 (1989) 299–308.
[4] G.J.M. Bruin, A.C. van Asten, X. Xu, H. Poppe, J. Chromatogr. 608 (1992) 97–107.
[5] W.G. Kuhr, E.S. Yeung, Anal. Chem. 60 (1988) 1832–1834.
[6] S. Mho, E.S. Yeung, Anal. Chem. 57 (1985) 2253–2256.
[7] W.D. Pfeffer, T. Takeuchi, E.S. Yeung, Chromatographia 24 (1987) 123–126.
[8] W.G. Kuhr, E.S. Yeung, Anal. Chem. 60 (1988) 2642–2646.
[9] P.E. Andersson, W.D. Pfeffer, L.G. Blomberg, J. Chromatogr. A 699 (1995) 323–330.
[10] T.W. Garner, E.S. Yeung, J. Chromatogr. 515 (1990) 639–644.
[11] T. Wang, R. Hartwick, J. Chromatogr. 607 (1992) 119–125.
[12] X. Xu, W.Th. Kok, H. Poppe, J. Chromatogr. A 716 (1995) 231–240.
[13] X. Xu, W.Th. Kok, J.C. Kraak, H. Poppe, J. Chromatogr. B 661 (1994) 35–45.
[14] C.L. Colyer, K.B. Oldham, A.V. Sokirko, Anal. Chem. 67 (1996) 3234.
[15] C.L. Colyer, K.B. Oldham, J. Chromatogr. A 716 (1996) 3.
[16] M.S. Bello, P. de Besi, P.G. Righetti, J. Chromatogr. A 652 (1993) 317–327.
[17] H. Poppe, J. Chromatogr. 506 (1990) 45.
[18] H. Poppe, Anal. Chem. 64 (1992) 1908–1919.
[19] X. Xu, W.Th. Kok, H. Poppe, J. Chromatogr. A 742 (1966) 211–227.
[20] T. Wang, R.A. Hartwick, J. Chromatogr. 589 (1992) 307–313.
[21] J.N. van der Moolen, H. Poppe and H.C. Smit, Anal. Chem, submitted for publication.
[22] T. Hirokawa, M. Nishino, N. Aoki, Y. Sawamoto, T. Yagi, J. Akiyama, J. Chromatogr. 271 (1983) D1–D106.
[23] T. Hirokawa, Y. Kiso, J. Chromatogr. 628 (1993) 283–308.
[24] T. Hirokawa, S. Kobayashi, Y. Kiso, J. Chromatogr. 318 (1985) 195.
[25] G. Kortüm, W. Vogel, K. Andrussow, Dissociation Constants of Organic Acids in Aqueous Solution, Butterworths, London, 1961.
[26] D.D. Perrin, Dissociation Constants of Organic Bases in Aqueous Solution, Butterworths, London, 1965.